Three-Dimensionally Ordered Macroporous Li 4 Ti 5 O 12 : Effect of Wall Structure on Electrochemical Properties

ARTICLE *in* CHEMISTRY OF MATERIALS · MARCH 2006

Impact Factor: 8.35 · DOI: 10.1021/cm052203y

Three-Dimensionally Ordered Macroporous $Li_4Ti_5O_{12}$: Effect of Wall Structure on Electrochemical Properties

Erin M. Sorensen,[†] Scott J. Barry,[†] Ha-Kyun Jung,[§] James R. Rondinelli,[#] John T. Vaughey,[‡] and Kenneth R. Poeppelmeier*,[†]

Department of Chemistry, Northwestern University, Evanston, Illinois 60208-3113, Advanced Materials Division, Korea Research Institute of Chemical Technology, Yuseong, Daejeon, South Korea, Materials Science and Engineering Department, Northwestern University, Evanston, Illinois 60208-3108, Chemical Engineering Division, Argonne National Laboratory, Illinois 87185-0755

Received October 4, 2005. Revised Manuscript Received November 18, 2005

Three-dimensionally ordered macroporous (3DOM) $Li_4Ti_5O_{12}$ was synthesized using poly(methyl methacrylate) colloidal crystal templates and metal organic aqueous precursors. 3DOM structures of various filling fractions and wall thicknesses were synthesized, and the materials evaluated in lithium ion battery cells. The 3DOM architecture was found to markedly improve the rate capability of $Li_4Ti_5O_{12}$ when the voids of the template were underfilled or perfectly filled. When the template voids were overfilled, the performance of the electrode was similar to that of nonporous $Li_4Ti_5O_{12}$. We believe the enhanced rate capability results from the interconnected network of nanometer scale walls, which create short lithium diffusion distances and better contact with the electrolyte. SEM and TEM micrographs reveal that the nature of the wall structure forms low angle grain boundaries in 3DOM $Li_4Ti_5O_{12}$, which enhances conduction pathways in the particle, especially at high rates.

Introduction

$Li_4Ti_5O_{12}$ is an appealing anode for lithium ion batteries. At 1.56 V, $Li_4Ti_5O_{12}$ inserts three lithium ions per formula unit, with a theoretical capacity of 175 mAh/ g. One of its most interesting properties is that lithium insertion occurs with very little expansion of its unit cell, which makes $Li_4Ti_5O_{12}$ a uniquely robust anode.[1−5] For most electrodes, notably main group metal based anodes such as tin, changes in crystallographic volume upon lithium insertion lead to particle isolation and capacity loss upon cycling, a key failure mechanism in lithium ion batteries.[6,7] In addition to its remarkable insertion properties, $Li_4Ti_5O_{12}$ also has excellent lithium ion mobility.[8] The combination of high lithium mobility and zero strain insertion properties make it an attractive anode for high rate battery applications.

High performance electrodes need to maintain high capacities as discharge rates are increased. In addition to materials properties, attributes such as particle size and morphology are also important and can be optimized. Spherical particle morphologies also minimize diffusion pathway lengths and allow for improved electrode properties owing to packing efficiencies. Modifications such as these can allow electrodes to sustain improved capacities at high discharge rates and retain high capacities even at extremely high discharge rates, e.g., 50C (complete discharge in 1.2 min).[9−11]

Significant effort has been devoted recently to producing smaller particles that have more active surface available for lithium insertion and should facilitate faster lithium diffusion owing to their shorter pathways. However, since a greater percentage of their active area is at the surface, undesirable reactions with the electrolyte, e.g., to form the solid electrolyte interphase layer, may result in higher fade rates as particles become coated and electronically isolated. Additionally, in most commercial battery systems, the separator used has approximately 1 μm diameter pores, so a nanoscale particle, if released from the electrode surface, may actually cross the barrier and agglomerate on the other electrode, resulting in capacity loss. An alternative approach to particle morphology design is to incorporate porosity into micrometer sized particles, thus maintaining good particle−

* To whom correspondence should be addressed. E-mail: krp@northwestern.edu.
[†] Dept of Chemistry, Northwestern University.
[§] Korea Research Institute of Chemical Technology.
[#] Materials Science and Engineering Dept, Northwestern University.
[‡] Argonne National Laboratory.

(1) Colbow, K. M.; Dahn, J. R.; Haering, R. R. *J. Power Sources* **1989**, *26*, 397−402.
(2) Ferg, E.; Gummow, R. J.; de Kock, A.; Thackeray, M. M. *J. Electrochem. Soc.* **1994**, *141*, L147−L150.
(3) Ohzuku, T.; Ueda, A.; Yamamoto, N. *J. Electrochem. Soc.* **1995**, *142*, 1431−1435.
(4) Panero, S.; Reale, P.; Ronci, F.; Albertini, V. R.; Scrosati, B. *Ionics* **2000**, *6*, 461−465.
(5) Peramunage, D.; Abraham, K. M. *J. Electrochem. Soc.* **1998**, *145*, 2609−2615.
(6) Aurbach, D.; Zaban, A.; Ein-Eli, Y.; Weissman, I.; Chusid, O.; Markovsky, B.; Levi, M.; Levi, E.; Schechter, A.; Granot, E. *J. Power Sources* **1997**, *68*, 91−98.
(7) Aurbach, D.; Zinigrad, E.; Cohen, Y.; Teller, H. *Solid State Ionics* **2002**, *148*, 405−416.
(8) Takai, S.; Kamata, M.; Fujine, S.; Yoneda, K.; Kanda, K.; Esaka, T. *Solid State Ionics* **1999**, *123*, 165−172.
(9) Kavan, L.; Prochazka, J.; Spitler, T. M.; Kalbac, M.; Zukalova, M.; Drezen, T.; Gratzel, M. *J. Electrochem.* Soc. **2003**, *150*, A1000−A1007.
(10) Kavan, L.; Gratzel, M. *Electrochem. Solid-State Lett.* **2002**, *5*, A39−A42.
(11) Amatucci, G. G. Nanostructure lithium titanate electrode for high cycle rate rechargeable electrochemical cell. US Patent Appl. 2,002,102,205, January 29, 2001.

10.1021/cm052203y CCC: $33.50
Published on Web 12/27/2005

particle contacts and adequate particle size, while maximizing the rate capability benefits of shorter diffusion pathways.[12]

A novel architecture that may improve the rate capability of electrode materials is the three-dimensionally ordered macroporous (3DOM) architecture.[13−16] While 3DOM based morphologies have garnered attention in the electrochemical community, the properties of these architectures have been of particular interest to the photonics community, owing to their ability to diffract visible light.[17,18] The photonics community has made major advancements in this area, typically using silica spheres for the template. Silica spheres can be annealed to strengthen the template by bonding the spheres together. The strengthened template is dip-coated with metal alkoxides, and the filled template is calcined to obtain the desired phase. To remove the template, it is etched using a weak HF solution. The resulting material is a uniform 3DOM structure with long range order.[19−24] When synthesized with silica spheres, these materials are similar to mineral opal in appearance and opalescence. The 3DOM architecture also can be created with spherical colloidal crystals of a polymer (e.g. poly(methyl methacrylate)) and sol−gel techniques. Precursors fill the void spaces in the template, and when the spheres are removed via heat or chemical leaching, an ordered macroporous structure is revealed constructed of the calcined precursor, be it a metal, metal oxide, or alloy.[19,23,25] Sol−gel syntheses have allowed numerous other oxide and non-oxide materials to be made in the inverse opal architecture, including CdS, CdSe, ZrO_2, and TiO_2 among others.[19,20,22−25]

The 3DOM structure, with an interconnected network of nanometer thick walls, is an attractive architecture for battery materials. The 3DOM architecture has two types of porosity: large macropores, on the order of 100 nm, formed by the spheres, and smaller mesopores, on the order of 15 nm, formed by contact points between the spheres. The surrounding walls of the 3DOM structure are not solid monoliths but consist of crystallites that form an irregular wall surface. Surface roughness works to the advantage of a battery electrode because it creates more defects for lithium to enter the electrode material. The porous walls increase the surface area and produce more surface sites for lithium to insert into the electrode material, while the nanometer thick walls shorten lithium diffusion distances, which reduces polarization within the electrode. While the 3DOM morphology within the particles produce short diffusion distances more typical of nanoparticles, the micrometer sized particles formed in the 3DOM synthesis ensure interparticle contact and electrode stability, which prevents particle isolation and thus capacity loss.[26−31]

Initial studies of electrodes made using materials with a 3DOM morphology have been shown to have improved performance; however, some studies designed to understand the effect of changes in the particle architecture itself are beginning to appear.[32] The effect of the 3DOM wall structure is not fully understood. Specifically, what effect does the wall structure of the 3DOM material have on the electrode performance? To further understand this effect, 3DOM lithium titanate has been synthesized using a single step metal organic precursor method. This method allows 3DOM $Li_4Ti_5O_{12}$ to be synthesized at different precursor loadings to create materials with a range of wall thicknesses. The resulting 3DOM lithium titanates have been characterized electrochemically in lithium cells to determine the effect of the 3DOM structure and the wall porosity on the rate capability of the electrode.

Experimental Section

All water used in the following synthetic steps was distilled and deionized to a resistivity of 18.2 MΩ·cm. All reagents were used as received without further purification.

Materials. $Li(CH_3COO)\cdot 2H_2O$ (99.999%, Aldrich), $TiCl_4$ (99.9%, Aldrich), $H_2C_2O_4\cdot 2H_2O$ (99% Sigma-Aldrich), 2,2′-azobis(2-methylpropionamidine) dihydrochloride (97% Aldrich), $K_2S_2O_8$ (97% Aldrich), methyl methacrylate (99% Sigma-Aldrich), polystyrene, (99% Sigma-Aldrich), and NH_4OH (29 vol %, Fisher) were used as received.

Template Synthesis. Non-cross-linked poly(methyl methacrylate) (PMMA) and polystyrene spheres (PS) were prepared by surfactant-free emulsion polymerization according to the literature using 2,2′-azobis(2-methylpropionamidine) dihydrochloride (Aldrich) or $K_2S_2O_8$ as the initiator.[20,33−35] Spheres with narrow distribution of diameters ca. 300 nm were synthesized. Prior to use, unreacted starting materials and impurities were removed by washing and centrifuging (9000 rpm for 40 min) the spheres in (1:1 v/v) dilute methanol. After being washed, the spheres were centrifuged again to achieve a cubic close packed template, and the liquid was evaporated in air under ambient conditions. Visual

(12) Martin, C. R.; Mitchell, D. T. *Electroanal. Chem.* **1999**, *21*, 1−74.
(13) Lytle, J. C.; Yan, H.; Ergang, N.; Smyrl, W. H.; Stein, A. *J. Mater. Chem.* **2004**, *14*, 1616−1622.
(14) Yan, H.; Sokolov, S.; Lytle, J. C.; Stein, A.; Zhang, F.; Smyrl, W. H. *J. Electrochem. Soc.* **2003**, *150*, A1102−A1107.
(15) Lee, K. T.; Lytle, J. C.; Ergang, N. S.; Oh, S. M.; Stein, A. *Adv. Funct. Mater.* **2005**, *15*, 547−556.
(16) Sakamoto, J. S.; Dunn, B. *J. Mater. Chem.* **2002**, *12*, 2859−2861.
(17) Yablonovitch, E. *Phys. Rev. Lett.* **1987**, *58*, 2059−2062.
(18) John, S. *Phys. Rev. Lett.* **1987**, *58*, 2486−2489.
(19) Schroden, R. C.; Al-Daous, M.; Stein, A. *Chem. Mater.* **2001**, *13*, 2945−2950.
(20) Schroden, R. C.; Al-Daous, M.; Blanford, C. F.; Stein, A. *Chem. Mater.* **2002**, *14*, 3305−3315.
(21) Stein, A. *Microporous Mesoporous Mater.* **2001**, *44*−*45*, 227−239.
(22) Meseguer, F.; Blanco, A.; Miguez, H.; Garcia-Santamaria, F.; Ibisate, M.; Lopez, C. *Colloids Surf., A* **2002**, *202*, 281−290.
(23) Stein, A.; Schroden, R. C. *Curr. Opin. Solid State Mater. Sci.* **2001**, *5*, 553−564 and references therein.
(24) Kuai, S.-L.; Bader, G.; Ashrit, P. V. *Appl. Phys. Lett.* **2005**, *86*, 221110/1−221110/3.
(25) Gaponenko, N. V. *Synth. Met.* **2001**, *124*, 125−130.
(26) Li, H.; Shi, L.; Lu, W.; Huang, X.; Chen, L. *J. Electrochem. Soc.* **2001**, *148*, A915−A922.
(27) Wu, X.; Li, H.; Chen, L.; Huang, X. *Solid State Ionics* **2002**, *149*, 185−192.
(28) Yoshitake, H.; Abe, K.; Kitakura, T.; Gong, J. B.; Lee, Y. S.; Nakamura, H.; Yoshio, M. *Chem. Lett.* **2003**, *32*, 134−135.
(29) Xu, K.; Zhang, S.; Jow, T. R. *Electrochem. Solid-State Lett.* **2003**, *6*, A117−A120.
(30) Zhang, S.; Ding, M. S.; Xu, K.; Allen, J.; Jow, T. R. *Electrochem. Solid-State Lett.* **2001**, *4*, A206−A208.
(31) Zhang, S. S.; Xu, K.; Jow, T. R. *J. Electrochem. Soc.* **2002**, *149*, A1521−A1526.
(32) Ergang, N. S.; Lytle, J. C.; Yan, H.; Stein, A. *J. Electrochem. Soc.* **2005**, *152*, A1989−A1995.
(33) Holland, B. T.; Blanford, C. F.; Do, T.; Stein, A. *Chem. Mater.* **1999**, *11*, 795−805.
(34) Zou, D.; Ma, S.; Guan, R.; Park, M.; Sun, L.; Aklonis, J. J.; Salovey, R. *J. Polym. Sci., Part A: Polym. Chem.* **1992**, *30*, 137−144.
(35) Goodwin, J. W.; Ottewill, R. H.; Pelton, R.; Vianello, G.; Yates, D. E. *Brit. Polym. J.* **1978**, *10*, 173−180.

observation of an iridescent array upon solvent evaporation indicated that the packing of spheres was highly ordered.

Precursor Synthesis. Titanyl oxalate preparation began with synthesis of aqueous $TiOCl_2$ from $TiCl_4$, as described in the literature.[36] Fresh $Ti(OH)_4$ was precipitated from the 49.6 mL of 2.017 M $TiOCl_2$ with 27 mL of aqueous NH_4OH. The precipitate was washed three times to remove excess NH_4OH and then combined with 25.5 g oxalic acid (0.202 mol) ($H_2C_2O_4 \cdot 2H_2O$) and water to form $H_2TiO(C_2O_4)_2$ in solution.[37] The lithium source was prepared by dissolving 25.5051 g of $Li(CH_3COO) \cdot 2H_2O$ (0.250 mol) in 250 mL of water. All the solutions were clear and were adjusted to 1 M of metal concentration. Upon combination of the two solutions, the precursor remained clear and no precipitate formed. A mixture (5:4 v/v) of titanyl oxalate solution and lithium acetate was used as a precursor solution for fabrication of 3DOM $Li_4Ti_5O_{12}$ electrode material.

3DOM Formation. Before the infiltration of precursor into the voids between PMMA or PS spheres, 20 vol % of methanol for the resulting solution was added in precursor solution to increase the wettability of the PMMA or PS sphere template. Three different precursor loading amounts were used to synthesize the three 3DOM $Li_4Ti_5O_{12}$ samples. For the 100% filling fraction, 11.6 mL of precursor solution was poured in a beaker containing 3.4 g of PMMA template. For the 75% filling fraction, 8.7 mL was used as the precursor, and for the 125% filling fraction, 14.5 mL was used. The beakers sat uncovered in air in order to solidify the composites. In this step, no swelling effect of the templates was observed. Finally, to eliminate the organic template and to form 3DOM materials, the composites were calcined in air at a muffle-type furnace under the heating rate of 2 °C/min to 675 °C held for 6 h at the temperature and cooled at a rate of 2 °C/min.

Product Analysis. Powder X-ray diffraction data was recorded on Rigaku ATX-G diffractometer with Ni-filtered Cu Kα radiation, operating at 50 kV and 240 mA. Data were collected in the 2θ range of 17° to 80° by scanning every 0.02° for 4.0 s. Scanning electron microscope work was performed on a Hitachi S-3500 SEM with an accelerating voltage of 3 kV and an emission current of 10 μA. SEM samples were attached to an aluminum mount using carbon tape and coated with 45 Å of Au/Pd. TEM samples were sonicated in methanol for 5 min and dispersed on a holey carbon grid. Transmission electron microscopy was performed on a Hitachi H-8100 TEM with an accelerating voltage of 200 kV and an emission current of 30 mA. TEM samples were sonicated in methanol for 5 min and dispersed on a holey carbon grid. TEM sample preparation of 100% and 125% filled samples did not result in sufficiently thin samples to be electron transparent.

Electrochemical Characterization. 3DOM $Li_4Ti_5O_{12}$ was finely ground to an average particle size of 5 μm and then mixed with 10 wt % acetylene black and 10 wt % polyvinylidenedifluoride (PvDF) binder. The electrode mixture was laminated with a doctor blade set to 200 μm onto copper foil and dried at 75 °C for 1 h in air and vacuum-dried for 1 h at 120 °C before use. 3DOM $Li_4Ti_5O_{12}$ was loaded to roughly 5.31 mg/cm^2 for all cells. Electrochemical cells were constructed in an argon-filled glovebox using lithium metal as the negative electrode. Cells were constructed using a Celgard 2400 separator and 1 M $LiPF_6$ in a 1:1 wt % mixture of ethylene carbonate (EC)/diethyl carbonate (DEC) electrolyte. Cells were cycled using constant current between 0.1 mA to 1 mA in the voltage window 1.2 and 3.2 V on a MacPile II galvanostat/potentiostat.

Results and Discussion

The morphology and surface area of particles within an electrode has a profound effect on the electrochemical properties of a material. By creating electrode materials with higher surface areas, the rate capability of many materials has been markedly improved. The primary means of increasing the surface-to-bulk ratio of the active electrode phase has been to decrease particle dimensions from micrometers to nanometers. While the rate capability of the electrode materials is improved with decreasing particle size, other concerns, such as electronic particle isolation owing to the formation of the solid electrolyte interphase layer or the effect of particles physically crossing or obstructing the separator, have come to the fore.[26,27,30,38]

The 3DOM architecture and local wall microstructure addresses the concern of rate capability and particle isolation. The micrometer sized 3DOM particles ensures that particles will be easier to process, remain in electrical contact, and do not diffuse through the separator during battery cycling, while the nanometer thick walls create sufficiently short diffusion paths and increase the available number of surface sites as in nanometer sized particles. In fact, V_2O_5 electrodes made by using materials with a 3DOM architecture has shown enhanced rate capability and greater cycleability when compared to a standard V_2O_5 material, while other 3DOM electrode materials have exhibited improvements in capacity retention.[13−16,32] Most of these materials, however, experience dramatic volume changes upon cycling, which contribute to the decline in capacity with cycling as the designed macrostructure collapses. For example, the capacity of a 3DOM SnO_2 electrode dropped precipitously with cycling because of the large volume expansion that occurred with lithium addition. After the initial cycle, the material had lost the inherent advantages of the initial 3DOM architecture.[13] Because $Li_4Ti_5O_{12}$ experiences little volume change with lithium insertion, the integrity of the 3DOM architecture should remain intact when cycled.

The structure of the $Li_4Ti_5O_{12}$ spinel consists of lithium and titanium atoms randomly distributed on one-half of the octahedral sites and lithium atoms filling one-eighth of the tetrahedral sites within the oxygen close packed lattice.[39] Expressing this distribution in spinel notation, the stoichiometry can be written as $Li[Li_{0.33}Ti_{1.67}]O_4$. As current is applied and lithium is passed, Ti^{4+} is reduced to Ti^{3+} within the octahedrally coordinated framework, allowing a topotactic transition between $Li_4Ti_5O_{12}$ and $Li_7Ti_5O_{12}$. The three inserted lithium ions and the tetrahedrally coordinated lithium ion move to occupy adjacent octahedral sites resulting in a layered rock salt phase, $Li_7Ti_5O_{12}$, via a two-phase reaction. Although substantial chemical changes occur during conversion between the two phases, the change in unit cell volume is roughly 0.3%.[40,41] See Figure 1.

The single step metal organic precursor method used to synthesize 3DOM $Li_4Ti_5O_{12}$ relies on capillary action to fill

(36) Park, S. D.; Cho, Y. H.; Kim, W. W.; Kim, S.-J. *J. Solid State Chem.* **1999**, *146*, 230−238.
(37) Clabaugh, W. S.; Swiggard, E. M.; Gilchrist, R. *J. Res. Natl. Bur. Stand.* **1956**, *56*, 289−91; Research Paper No 2677.
(38) Li, H.; Shi, L.; Wang, Q.; Chen, L.; Huang, X. *Solid State Ionics* **2002**, *148*, 247−258.
(39) Deschanvres, A.; Raveau, B.; Sekkal, Z. *Mater. Res. Bull.* **1971**, *6*, 699−704.
(40) Scharner, S.; Weppner, W.; Schmid-Beurmann, P. *J. Electrochem. Soc.* **1999**, *146*, 857−861.

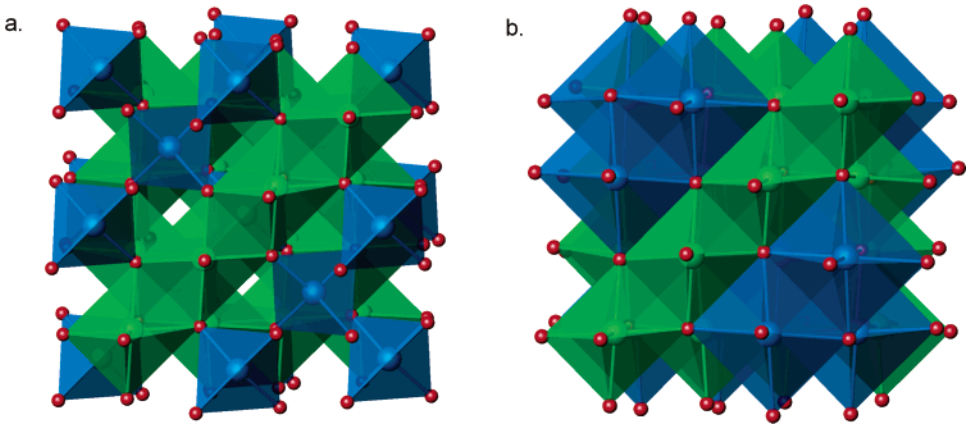

Figure 1. (a) $Li_4Ti_5O_{12}$ spinel structure type. Blue tetrahedra represent lithium, and green octahedra represent disordered lithium and titanium. (b) $Li_7Ti_5O_{12}$, rock salt. Blue octahedra represent lithium, and green octahedra represent disordered lithium and titanium.

the template. Aqueous solutions of lithium acetate and titanyl oxalate are combined in a 4:5 metal ion ratio outside of the template. Lithium acetate and titanyl oxalate were used as precursors for this synthesis because they are both water soluble, air stable, and can be combined without any detectable precipitation. Methanol is added to the combined precursors so that the aqueous precursors can wet the voids in the template. The solution is introduced slowly to the PMMA template, which imbibes the solution through capillary action. As excess water evaporates under ambient conditions, the slow evaporation of the solution continually equilibrates the metal ion presence within the voids. Generally, it would be expected that the precursors would crystallize on the sides of the evaporation vessel; however, this is not observed. In fact, when a dye is used to map precursor infiltration within the template, the dye is found to be uniformly distributed throughout the pieces of template. Single step infiltration allows 1−2 g of 3DOM $Li_4Ti_5O_{12}$ to be synthesized with uniform wall thicknesses and properties in one synthesis. The template voids are fully loaded with the metal precursors, which create a 3DOM structure with substantial walls. Capillary action is also used to incorporate metal alkoxides into polymer sphere templates.[33] With metal alkoxides, organic solvents used in the synthesis can lead to sphere swelling, where the spheres begin to swell with solvent. This swelling can break up the template and degrade the 3DOM morphology. Because the polymer template is not soluble in water, using it as the primary solvent prevents most swelling.

After drying, the filled templates are calcined to remove the polymer sphere template and convert the precursors to 3DOM $Li_4Ti_5O_{12}$. See Figure 2. As calcination time increases, grains of lithium titanate grow larger and, consequently, the 3DOM structure breaks down. However, lithium titanate benefits from long calcination times, because rutile and anatase are refractory oxides that do not easily react to form the desired phase. In addition to these concerns, lithia has a tendency to volatilize at temperatures greater than 700 °C. By calcining at 675 °C for 6 h, a uniform and reproducible 3DOM architecture is created. This 3DOM

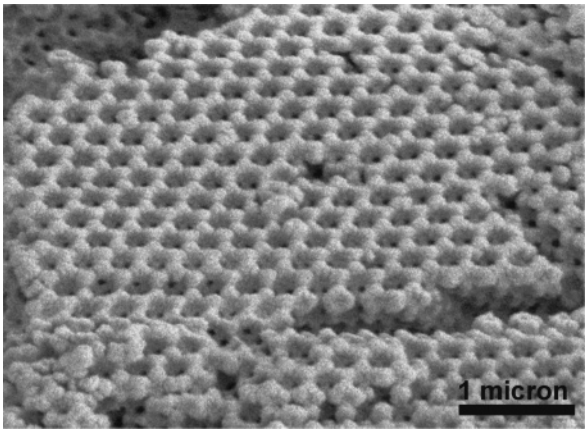

Figure 2. 3DOM $Li_4Ti_5O_{12}$ SEM micrograph.

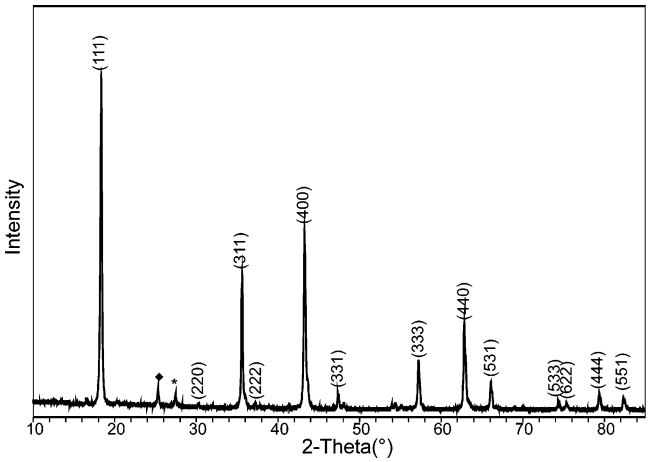

Figure 3. Powder X-ray diffraction pattern of 3DOM $Li_4Ti_5O_{12}$. The primary reflection of anatase at 25.3° is denoted by ♦, and the primary reflection of rutile at 27.5° is denoted by *.

architecture, however, comes at the expense of phase purity. In every case, the synthesis results in small amounts of Li_2TiO_3, rutile, and anatase as side products. See Figure 3. On the basis of Rietveld refinement to determine phase fractions, they were found to encompass approximately 10% of the total mass.[42−46] Even when additional lithium precursor is

(41) Ronci, F.; Reale, P.; Scrosati, B.; Panero, S.; Rossi Albertini, V.; Perfetti, P.; di Michiel, M.; Merino, J. M. *J. Phys. Chem. B* **2002**, *106*, 3082−3086.

(42) Larson, A. C.; Von Dreele, R. B. General Structure Analysis System (GSAS), 2000.
(43) Toby, B. H. *J. Appl. Crystallogr.* **2001**, *34*, 210−213.
(44) Gualtieri, A. F. *J. Appl. Crystallogr.* **2000**, *33*, 267−278.
(45) Gualtieri, A. F.; Brignoli, G. *J. Appl. Crystallogr.* **2004**, *37*, 8−13.

added, the amount of titania phases does not decrease, which indicates lithia volatility is not a factor in the inhomogeneity of the product. Additionally, if the dried precursors are calcined outside of the polymer template, pure lithium titanate can be achieved.

The presence of Li_2TiO_3, rutile, and anatase in the final 3DOM $Li_4Ti_5O_{12}$ product is not easily ascribed to one single factor; rather, a confluence of factors combines to bring about conditions that create these side products, including dried precursor composition, polymer sphere composition, and polymerization initiators. The various templates, e.g., azo initiated PS or KPS initiated PMMA, resulted in different amounts of TiO_2 presence. Qualitatively, the most impurities were found when the templates were made from KPS initiated PS, while the least resulted from azo-initiated PMMA template. While PS and PMMA decompose around the same temperature, 350 °C, the decomposition processes for these two polymers are different. Local temperatures in the template can exceed 700 °C, which may cause lithia to volatilize. As discussed previously, however, excess lithium did not reduce the TiO_2 fraction present in the final product. Another possibility includes the interactions between the sphere surface and the precursor, which could cause segregation of the metal ions. For example, the polymerization initiator terminates the surface of the sphere; thus, the void space of the template can be considered negatively or positively charged. The sulfate terminated spheres are negatively charged on the surface, while the azo terminated spheres are positively charged.[47] In addition to cationic and anionic differences on the sphere surface, the basicity of the surface is different. The azo initiated surface terminates in a basic alkylamine, while the KPS initiated surface terminates in a weakly basic sulfate group.

In addition to interactions between the template surface and the precursors, the composition of the dried precursors within the template voids also may contribute to the formation of side products. Although the speciation of the combined precursors in solution is not known, upon drying, the phase $Li_2[TiO(C_2O_4)_2]\cdot 4H_2O$ is detected in the template with powder X-ray diffraction.[48] Alkali metal titanyl oxalates consists of a square of four titanium atoms linked by bridging oxygen atoms.[49−52] Each titanium cation's coordination sphere is filled by two bidentate oxalate groups. Such clusters carry a charge of 8^-, which is compensated by the alkali metals. See Figure 4. Although these tetramers are not observed in dilute solutions, they most likely condense as the solution concentrates with evaporation, and, with crystallization, segregation of the metallic species within the

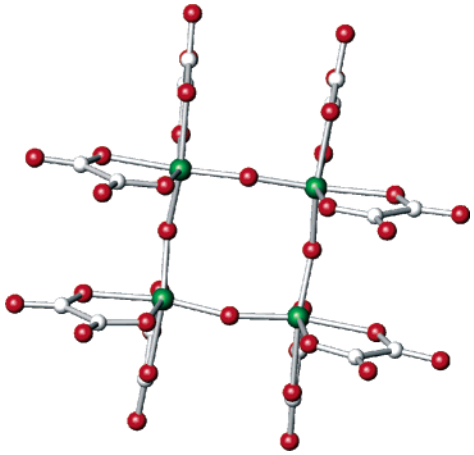

Figure 4. Titanyl oxalate ring. Green spheres represent titanium, white spheres represent carbon, and red spheres represent oxygen.

template occurs. In some voids, the paucity of lithium may be one of the causes of rutile and anatase formation, while in other voids, the lithium excess leads to the formation of Li_2TiO_3. The confluence of a crystallized precursor composition with a 2:1 Li:Ti ratio and interactions between surface species and the precursors may lead to the persistent presence of both Li_2TiO_3 and titania phases as side products in the synthesis of 3DOM $Li_4Ti_5O_{12}$.

To understand the effects of 3DOM wall structure on the electrochemical properties of 3DOM $Li_4Ti_5O_{12}$, three different 3DOM samples were synthesized. The first 3DOM sample was synthesized such that the template voids were entirely filled with precursors when dried. To calculate how many moles of precursor will fill the template voids, the total void volume available in the template is first determined. The template mass is converted to volume with the polymer density; in this case, the density of PMMA is 1.19 g/mL.[53] The colloidal crystal template packs in a cubic close packed manner, so the void space is 26% of the total template volume.[54−59] With the tap density of the dried precursors (1.8 g/mL), it is then possible to calculate the moles of precursor required to fill the void space completely. 3DOM $Li_4Ti_5O_{12}$ synthesized by this technique is considered to be 100% precursor loading. To synthesize 3DOM $Li_4Ti_5O_{12}$ at a range of filling fractions, the amount of precursors loaded into the template was varied. In the second sample, the template voids were underfilled to 75%, to create a more porous wall structure, rather than completely loaded with dried precursors in the first case. The third sample overfilled the voids to form a less porous wall structure. The precursor loading in this less porous sample was 125%.

The nature of the walls within the 3DOM particles themselves changes with precursor loading amounts. As the

(46) Rietveld, H. M. *Acta Crystallogr.* **1967**, *22*, 151−152.
(47) Penboss, I. A.; Napper, D. H.; Gilbert, R. G. *J. Chem. Soc., Faraday Trans. 1* **1983**, *79*, 1257−1271.
(48) Fester, A. *Titan-Sauerstoff-Koordination in Titanylverbindungen.* Johann Wolfgang Goethe-Universität Frankfurt am Main: Frankfurt, 1990 (English title: *Titanium Oxygen Coordination in Titanyl Complexes*).
(49) Van de Velde, G. M. H.; Harkema, S.; Gellings, P. J. *Inorg. Chim. Acta* **1974**, *11*, 243−252.
(50) Brisse, F.; Haddad, M. *Inorg. Chim. Acta* **1977**, *24*, 173−177.
(51) Fester, A.; Bensch, W.; Troemel, M. *Inorg. Chim. Acta* **1992**, *193*, 99−103.
(52) Fester, A.; Bensch, W.; Troemel, M. *Acta Crystallogr., Sect. C: Cryst. Struct. Commun.* **1994**, *C50*, 850−852.
(53) Bruno, T. J.; Svoronos, P. D. N. In *Handbook of Basic Tables for Chemical Analysis*, 2nd ed; CRC Press: New York, 2003; p 584.
(54) Carlson, R. J.; Asher, S. A. *Appl. Spectrosc.* **1984**, *38*, 297−304.
(55) Miguez, H.; Meseguer, F.; Lopez, C.; Mifsud, A.; Moya, J. S.; Vazquez, L. *Langmuir* **1997**, *13*, 6009−6011.
(56) Vos, W. L.; Megens, M.; van Kats, C. M.; Boesecke, P. *Langmuir* **1997**, *13*, 6004−6008.
(57) van Blaaderen, A.; Rue, R.; Wiltzius, P. *Nature (London)* **1997**, *385*, 321−324.
(58) Woodcock, L. V. *Nature (London)* **1997**, *385*, 141−143.
(59) Larsen, A. E.; Grier, D. G. *Nature (London)* **1997**, *385*, 230−233.

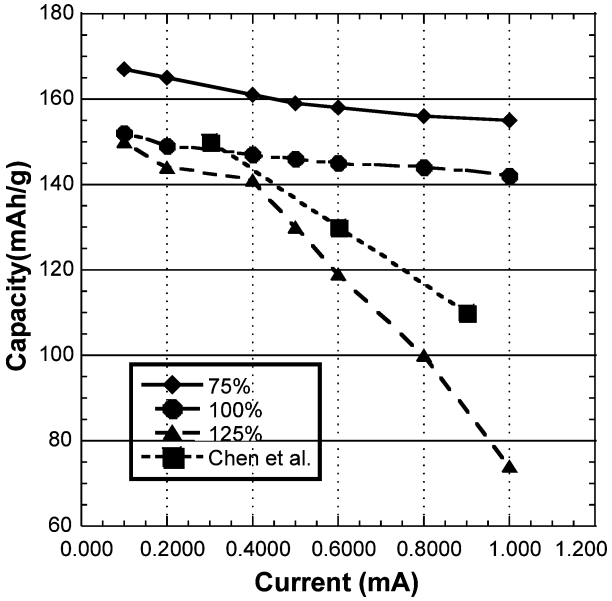

Figure 5. Capacity plots of 75%, 100%, 125% void filling 3DOM $Li_4Ti_5O_{12}$ at increasing current densities. Comparison data from ref 55.

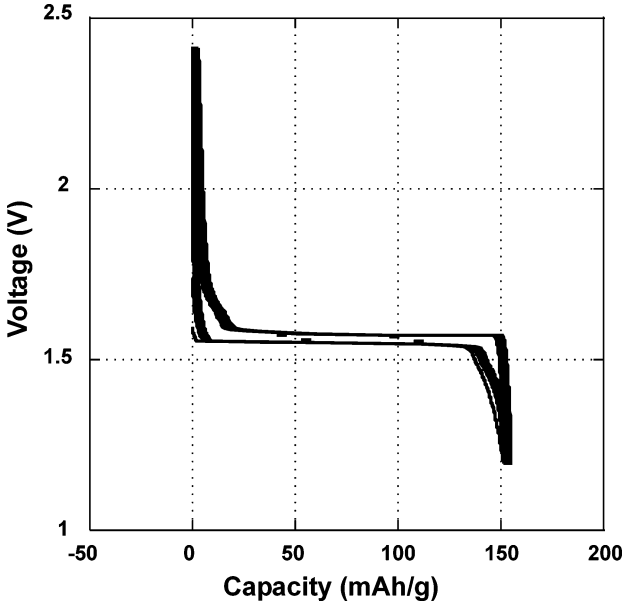

Figure 6. Capacity plot of 100% void filling 3DOM $Li_4Ti_5O_{12}$ at 0.1 mA. Ten cycles shown.

precursors' loading changes, the size of the crystallites that build the walls does not change, since their growth is governed by solid state diffusion processes when calcined. Rather, the number of crystallites and the number of contact points between the crystallites change according to the filling fraction, and thus the wall porosity varies as well. The porosity created by the macropores could be altered by changing sphere size; however, the size of the pores is so large relative to the electrochemical diffusion processes that they do not grossly affect the performance of the electrode. 3DOM structures with different filling fractions allow the combined effects of surface roughness, wall thickness, and mesopores upon capacity performance to be understood.

To determine the rate capability of 3DOM $Li_4Ti_5O_{12}$, electrodes made from these materials were cycled at increasing current densities. As with any electrode material, the capacity decreases with increasing current density; however, the maintenance of the capacity is affected by the morphology of the active material. In the case of $Li_4Ti_5O_{12}$, lithium insertion is accompanied by movement of the tetrahedrally coordinated lithium atom in the unit cell. By drawing more current from the battery, the lithium ions must move more quickly from anode to electrolyte to cathode; however, within the spinel phase, solid state diffusion processes do not accelerate. Lithium ion mobility is an inherent temperature-dependent property of a material; thus, shortening diffusion distances is the main method to alleviate diffusion related limitations. Increasing surface area also creates more defect sites for lithium to enter the active material.

3DOM $Li_4Ti_5O_{12}$ synthesized with 100% precursor loading was cycled at several charge densities to determine the capacity of these materials. At slow discharge rates, 3DOM lithium titanate performs slightly better than most nonporous ceramic forms of $Li_4Ti_5O_{12}$, and as the rate increases, the capacity of the material falls off only slightly. See Figure 5. At 0.1 mA or 0.063 mA/cm^2 current density, 3DOM lithium titanate has a specific capacity of 152 mAh/g, in good agreement with literature values with reported specific capacities of nonporous $Li_4Ti_5O_{12}$, in the range of 140−150 mAh/ g.[4,5,60−65] See Figure 6. Only minor improvements in capacity are expected, since at slower rates, lithium ions have more time to diffuse into particles and capacity at low rates is not diffusion limited. As the discharge rate increases, the capacity of 3DOM $Li_4Ti_5O_{12}$ decreases. The specific capacity of 3DOM $Li_4Ti_5O_{12}$ at 0.2 mA (0.125 mA/cm^2) is 149 mAh/ g. Even though the rate of discharge has doubled, the capacity of the electrode has not really changed. At 1.0 mA (0.63 mA/cm^2), the capacity of 3DOM $Li_4Ti_5O_{12}$ is 143 mAh/g, which is 94% of the capacity observed at the slowest rate. See Figure 7. Nonporous lithium titanate has reported capacities of 100 mAh/g or less at similar current densities. The 3DOM structure at 100% precursor loading has shorter diffusion distances owing to the nanometer scale walls. At faster discharge rates, the short diffusion distances allow more lithium to reach the electrode bulk. Because the material has such a limited volume expansion over its whole stoichiometric range, the 3DOM structure was found to be intact even after 70 cycles. Thus the benefit of the 3DOM architecture is maintained under electrochemical charge and discharge. See Figure 8.

3DOM $Li_4Ti_5O_{12}$ exhibits superior rate capability compared to nonporous $Li_4Ti_5O_{12}$ at 100% precursor loading, but to explore the effect of interior wall structure upon the performance of $Li_4Ti_5O_{12}$, two additional 3DOM $Li_4Ti_5O_{12}$ materials were evaluated. When the precursors are loaded

(60) Chen, C. H.; Vaughey, J. T.; Jansen, A. N.; Dees, D. W.; Kahaian, A. J.; Goacher, T.; Thackeray, M. M. *J. Electrochem. Soc.* **2001**, *148*, A102−A104.
(61) Zaghib, K.; Simoneau, M.; Armand, M.; Gauthier, M. *J. Power Sources* **1999**, *81*−*82*, 300−305.
(62) Wang, G. X.; Bradhurst, D. H.; Dou, S. X.; Liu, H. K. *J. Power Sources* **1999**, *83*, 156−161.
(63) Shen, C.-m.; Zhang, X.-g.; Zhou, Y.-k.; Li, H.-l. *Mater. Chem. Phys.* **2003**, *78*, 437−441.
(64) Rho, Y. H.; Kanamura, K.; Umegaki, T. *Chem. Lett.* **2001**, 1322−1323.
(65) Peramunage, D.; Abraham, K. M. *J. Electrochem. Soc.* **1998**, *145*, 2615−2622.

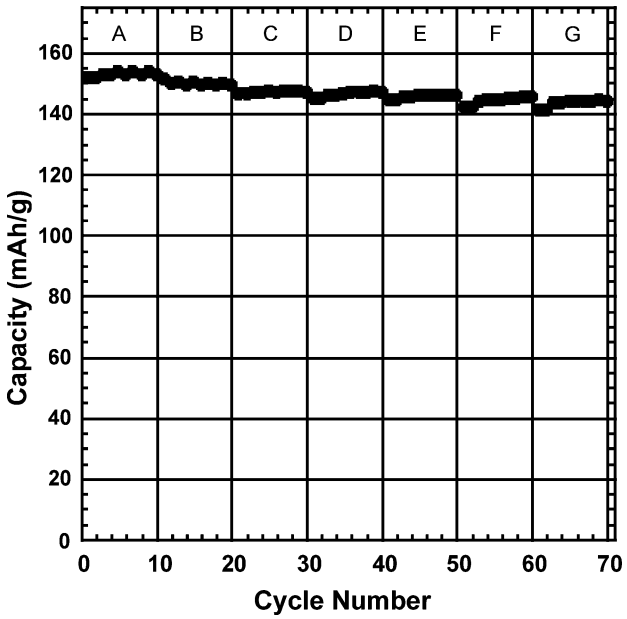

Figure 7. Capacity performance summary of 100% void filling 3DOM $Li_4Ti_5O_{12}$. A: 0.0625 mA/cm^2. B: 0.125 mA/cm^2. C: 0.250 mA/cm^2. D: 0.312 mA/cm^2. E: 0.375 mA/cm^2. F: 0.500 mA/cm^2. G: 0.625 mA/cm^2.

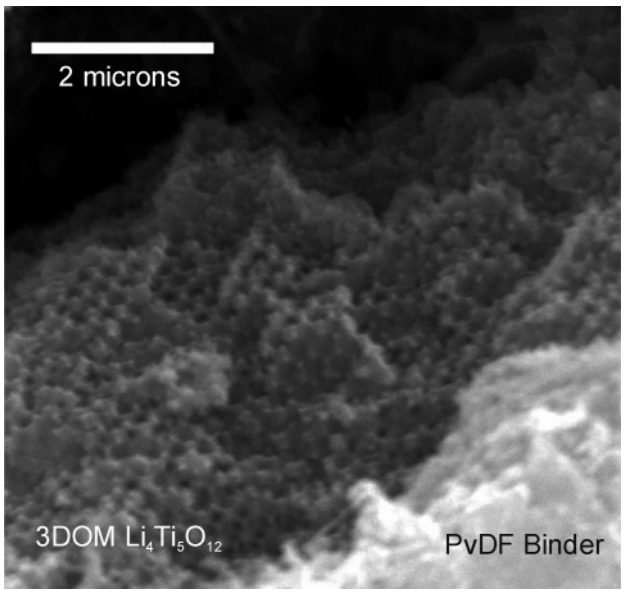

Figure 8. SEM micrograph of 100% void filling 3DOM $Li_4Ti_5O_{12}$ after 70 cycles.

into the template such that the filling is 125%, the porosity of the 3DOM walls is severely diminished. The initial capacity is similar to that seen in 100% filled 3DOM $Li_4Ti_5O_{12}$ at 150 mAh/g. As current density increases, the capacity decreases precipitously, with the average capacity at 0.63 mA/cm^2 only reaching 74 mAh/g. See Figure 5. The 125% filled 3DOM $Li_4Ti_5O_{12}$ behaves more like nonporous ceramic $Li_4Ti_5O_{12}$, rather than the enhanced rate capability demonstrated by 3DOM $Li_4Ti_5O_{12}$. Capacity decay with cycling is also observed in 125% filling electrode. At higher rates, the capacity decreases with each cycle, which is unusual for $Li_4Ti_5O_{12}$ based electrodes. See Figure 9. Typically, such capacity loss during cycling occurs with structural degradation of the electrode material, for example with SnO_2.[66−68] $Li_4Ti_5O_{12}$ does not suffer from structural decomposition upon lithium insertion, and in fact, at slower

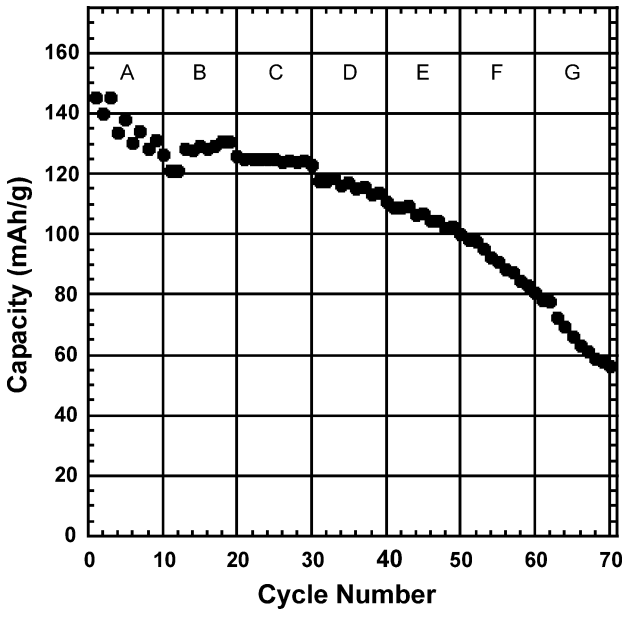

Figure 9. Capacity performance summary of 125% void filling 3DOM $Li_4Ti_5O_{12}$. A: 0.0625 mA/cm^2. B: 0.125 mA/cm^2. C: 0.250 mA/cm^2. D: 0.312 mA/cm^2. E: 0.375 mA/cm^2. F: 0.500 mA/cm^2. G: 0.625 mA/cm^2.

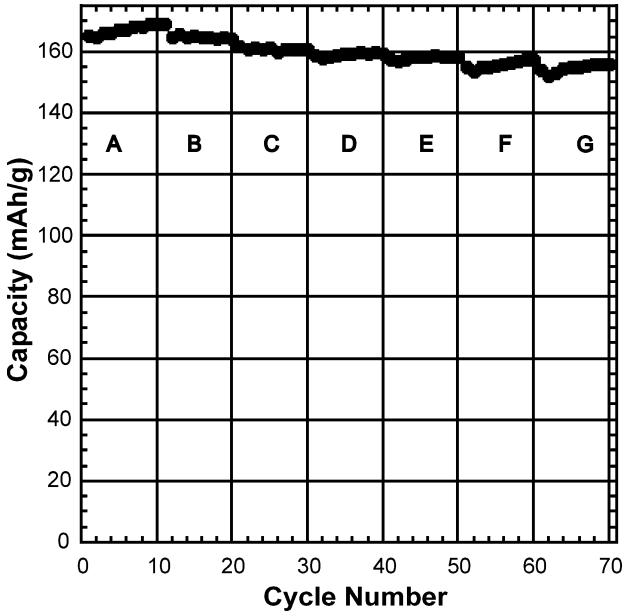

Figure 10. Capacity performance summary of 75% void filling 3DOM $Li_4Ti_5O_{12}$. A: 0.0625 mA/cm^2. B: 0.125 mA/cm^2. C: 0.250 mA/cm^2. D: 0.312 mA/cm^2. E: 0.375 mA/cm^2. F: 0.500 mA/cm^2. G: 0.625 mA/cm^2.

rates, these 125% filled electrodes maintained their capacity throughout each 10 cycle test. Capacity decay observed at higher rates indicates that the lithium insertion is impeded. Polarization within the electrode causes lithium to remain trapped in the electrode as each cycle ends, or else active material is lost from or electronically isolated within the electrode. In fact, the former is true, because upon resting, the electrode cycled again at 0.1 mA achieves 150 mAh/g.

The final 3DOM $Li_4Ti_5O_{12}$ was synthesized with 75% precursor loading. With underfilled voids, the 3DOM structure is even more porous than the 100% filled material and has shorter diffusion distances for lithium insertion. The initial capacity at 0.1 mA is closer to the theoretical capacity, at 167 mAh/g, and as discharge rate increases, the electrode

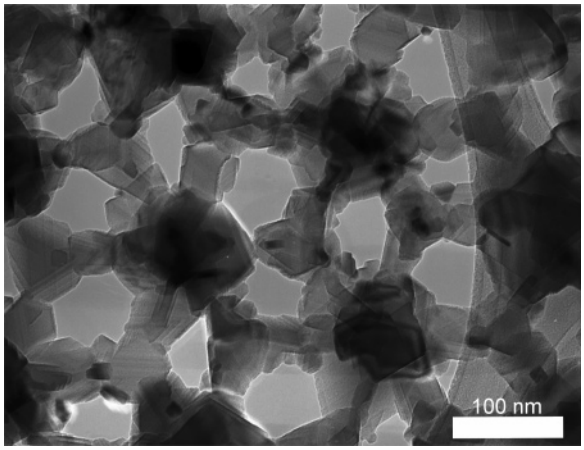

Figure 11. Wall structure of 75% filled 3DOM $Li_4Ti_5O_{12}$ illustrating low angle grain boundaries. TEM micrograph.

exhibits excellent capacity maintenance. At the maximum discharge rate using a current density of 0.63 mA/cm^2, the capacity is 155 mAh/g, higher than most reported capacities of nonporous Li_4TiO_{12} at 0.063 mA/cm^2.[4,5,61−65] See Figure 5. Enhanced porosity combined with short diffusion distances creates ideal circumstances for lithium insertion. As with the 100% filled 3DOM Li_4TiO_{12}, the 75% filled sample capacity remains steady throughout cycling and does not decay. See Figure 10.

The differences in capacity performance between the three 3DOM $Li_4Ti_5O_{12}$ electrodes elucidate the basis of the enhanced performance. The macroporous structure allows the electrolyte to penetrate every part of the 3DOM particle, which exposes more surfaces to insertion, while the internal wall structure produces a roughened surface. As current is applied, current flow is limited by lithium diffusion through the particle. The roughened, porous 3DOM wall has more sites for lithium ions to enter the electrode, which grows in importance as current increases. The increased surface-to-bulk ratio also makes high rate lithium insertion more facile, which in turn decreases polarization in the electrode.

The wall structure of the 75% filled 3DOM electrode also facilitates lithium insertion and electrical conduction in the particles. As seen in Figure 11, the crystallites that form the walls are not uniform in size; they are, however, connected such that the grain boundaries meet at low angles. Although not frequently discussed in relation to batteries, low angle grain boundaries are critical features in expediting electrical conductivity.[69] The low angle grain boundaries found in the 3DOM wall structure help to decrease polarization within the electrode by creating conduction pathways for the electrons.

The 3DOM structure allows more facile lithium diffusion at higher current densities owing to increased surface sites in the electrode. The shorter diffusion distances within the 3DOM walls also enhance the rate capability of the material. The reduced wall porosity in the 125% filled sample adversely affects the capacity maintenance of the electrode. As the thickness of the walls increases and the internal wall porosity decreases, polarization increases and lithium insertion is impeded. On the other hand, the porous walls in the 75% filled 3DOM structure lead to the highest capacities at our highest current densities, and these high capacities are maintained, which illustrates the utility of wall porosity to electrode performance.

Conclusion

Three-dimensionally ordered $Li_4Ti_5O_{12}$ was synthesized using lithium acetate and titanyl oxalate. By soaking the template in the combined precursor solution, total template void filling was achieved. This technique also allowed 3DOM $Li_4Ti_5O_{12}$ of different filling fractions to be synthesized. These synthesized materials were tested as anodes for lithium ion batteries, and their rate capability was determined. Those 3DOM electrodes with lower filling fractions, and thus more porous internal wall structures, demonstrated excellent rate capability and extremely high capacities in general. As wall porosity decreased, the rate performance of the electrode decreased. In the least porous sample, rate behavior was more like a nonporous solid, rather than a macroporous solid.

Acknowledgment. The authors gratefully acknowledge support from the Office of Naval Research (MURI Grant N00014-01-1-0810) and made use of the Central Facilities supported by the MRSEC program of the National Science Foundation (DMR-0076097) at the Materials Research Center of Northwestern University. Financial support from the Office of Basic Energy Sciences and the Office of FreedomCar and Vehicle Technologies of the U.S. Department of Energy under Contract No. W31-109-Eng-38 is also gratefully acknowledged. The submitted manuscript has been created by the University of Chicago as Operator of Argonne National Laboratory ("Argonne") under Contract No. W-31-109-ENG-38 with the U.S. Department of Energy. The U.S. Government retains for itself, and others acting on its behalf, a paid-up, nonexclusive, irrevocable worldwide license in said article to reproduce, prepare derivative works, distribute copies to the public, and perform publicly and display publicly, by or on behalf of the Government. The authors also thank Andreas Stein for fruitful discussions during the course of this work and with regard to this manuscript.

Supporting Information Available: Quantitative phase analysis of 3DOM $Li_4Ti_5O_{12}$ calculated using GSAS and EXPGUI software (PDF). This material is available free of charge via the Internet at http://pubs.acs.org.

CM052203Y

(66) Courtney, I. A.; Dahn, J. R. *Prog. Batt. Batt. Mater.* **1997**, *16*, 214−236.
(67) Courtney, I. A.; Dahn, J. R. *J. Electrochem. Soc.* **1997**, *144*, 2943−2948.
(68) Courtney, I. A.; Dahn, J. R. *J. Electrochem. Soc.* **1997**, *144*, 2045−2052.
(69) Evetts, J. E. *Supercond. Sci. Technol.* **2004**, *17*, S315−S318.